Calibration of an imaging system for monitoring light pollution from small UAVs

Pietro Fiorentin, Carlo Bettanini, Damiano Bogoni
Department of Industrial Engineering
University of Padova
Padova, Italy
pietro.fiorentin@unipd.it

Alessio Aboudan, Giacomo Colombatti,
University of Padova-CISAS "Giuseppe Colombo"
Padova, Italy

***Abstract*— The paper presents the calibration activity of the imaging system of an autonomous sensor suite designed for monitoring light pollution which, thanks to its extremely compact design, can be carried by drones or small balloons. Drones and air balloons can in fact play an important role in completing light emission measurement from satellites, allowing an increased spatial and time resolution from convenient altitudes and positions. The proposed sensor suite is able to measure the luminous intensity of polluting sources and their spectral power density with a wavelength resolution which allows to identify the different lamp technology used in street lighting. By operating over a limited area, the spatial resolution can be about tenths of meter and the time evolution of the luminosity can be measured over hours. The expected performance of imaging system has been verified through an extensive laboratory test activity allowing calibration with referenced light sources. The calibration of the multi-luminance meter allows measurements with a base uncertainty of about 5% of the reading. The multi-spectrometer has a FWHM equal to 10 nm and is able to measure the power density of the outdoor light source in the range between 400 nm and 700 nm.**

Keywords— imaging system; light pollution; artificial lighting; urban analysis; remote sensing;photometry; spectral analysis; UAV

I. INTRODUCTION

Outdoor lighting is required to increase safety on motorized roads, cycle tracks and pedestrian zones, in roads parking lots, in working places. It allows a better use of public spaces. As a counterpart it causes light pollution, the artificial luminance of the sky. It is not only an astronomical question, but also an alteration of the sensitive environmental balance [1].

Images from Earth-observing satellites were used to analyzed upward light, even if sensors had not a radiometric calibration [2]. Satellites with calibrated sensors highly improved the analysis [3-5]. But satellites had a poor horizontal spatial resolution of about 5 km [6].

The Visible Infrared Imaging Radiometer Suite Day-Night Band (VIIRS DNB) [7] allowed a horizontal resolution up to about 0.6 m and its wavelength responsivity is between 500 nm to 900 nm.

In any case, data from satellites present limitations. The spectral response of their radiometric sensor does not allow to discriminate "white" light sources. City light is not constant during the night, on the contrary it changes dynamically. Asynchronous satellite observations cannot follow this time evolution. Satellite photos are taken at nadir, while it is of interest to know how the emission varies with the observing angle.

Aerial observations can provide data from closer view than satellites [8-10]. Aerial surveys allow measurements of light emission at the zenith of the sources. This limits their efficacy as light pollution modelling requires the knowledge of light emitted in any direction and at any wavelength [11-13].

Drones and air balloons can allow to overcome limit of satellites and aerial acquisitions. The measuring system MINLU here presented can be carried on by unmanned aerial vehicle [14]. It deals with the upward emission of outdoor lighting, allowing the identification of the most important polluting light sources.

The paper describes briefly MINLU structure and the main features of the three cameras used for the acquisition. Also a spectrometer can be included in MINLU to measure the average power spectral density of the upward emitted light. The paper is focused on the description of the calibration procedures of the image luminance meter and of the image spectrometer and their obtained performances. The first measurements of these two instruments are presented under different light sources. We are preparing the first fly, it will allow to understand how the images of the framed light sources are influenced by the motion of the drone and if actions have to be considered to compensate the effect. Furthermore, up to now the relationships among the images from the three cameras are defined manually, a partial automatic identification of common framed light sources is foreseen for the future.

II. MINLU INSTRUMENT

MINLU is a completely autonomous imaging system commanded by a Central Data Management Unit (CDMU). The on boards electronics allows sensor conditioning, data acquisition, compression and storage. A digital hub connects the CDMU to the imaging subsystem; it is composed by three

978-1-7281-1344-9/19/$31.00 ©2019 IEEE

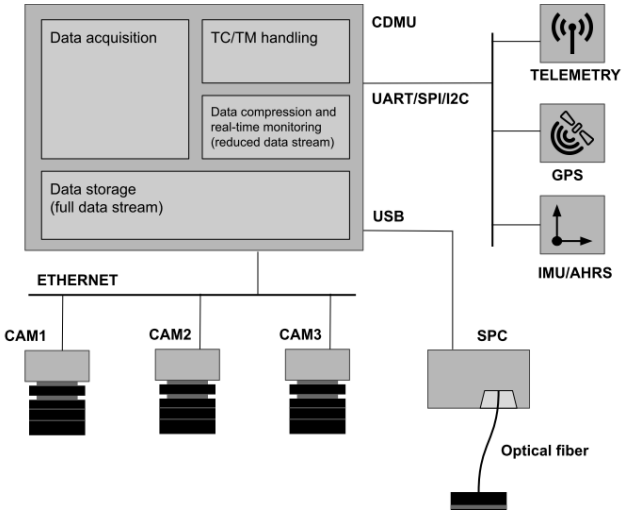

Fig. 1. MINLU architecture: Command and Data Management Unit (CDMU) is responsible for the synchronous data acquisition, data storage and real-time data preview. Acquired data is correlated with system position and attitude and saved on-board. Images are properly decimated, subsampled, compressed and sent back to ground in real-time. All the acquisition parameters can be configured throught proper telecommands.

cameras. A spectrometer completes the set of instruments devoted to light measurements. Telemetry is transmitted to ground through a Zigbee system. It includes acquired images, position and attitude information. Rechargeable lithium batteries provide the power to the whole system. A sketch of MILU is presented in figure 1.

Three digital cameras using the Sony STARVIS CMOS acquire the images. The sensor is a back illuminated one, improving the system sensitivity. The sensor size is 7.4 mm x 5 mm, its resolution is 3088 horizontal pixels x 2064 vertical pixels. The sensor specifications are presented in detail in table I.

A Theia ML410M f/1.4 lens is used for each of the three cameras. Using a focal length equal to 4 mm the field of view of the system is about 90°. The system can analyze upward emitted rays which are away from the nadir direction up to more than 45°. This ability greatly enhances opportunities in the study of upward-emitting light sources, particularly with respect to satellite measurements. Moving horizontally the acquisition system allows to measure the distribution of the luminous intensity of the same light source along most of the direction of the upward hemisphere. When the system flies at 200 m of altitude the cameras frame a surface 360m x 240m. In this condition the horizontal resolution at ground level is about 0.2 m.

Table I: Main specifications of the two kind of camera

Camera	acA3088-16gm	acA3088-16gc
Sensor name	IMX178LLJ-C	IMX178LQJ-C
Sensor type	CMOS	
shutter	rolling	
mono/color	Mono	color
Resolution (H x V Pixels)	3088 x 2064	
Optical size	1/1.8”	
Effective Sensor Diagonal	8.92 mm	
Pixel Size (H x V)	2.4 µm x 2.4 µm	
Image Data Interface	Gigabit Ethernet (1000 Mbit/s)	

An RGB camera will document the framed scene. The two others cameras use a monochromatic sensor. One camera works as a luminance meter and has an optical filter in front of its lens. A visible transmission diffracting grid is paced in front of the lens of the last camera. It converts the camera into a raw multi-spectrometer. Its wavelength resolution is about 2 nm, which is sufficient to identify different lighting sources.

A Stellarnet Black Comet spectrometer completes the set of light instruments. It is devoted to measure the total upward spectral radiance, emitted from light sources and lit surfaces. The instrument is optimized to measure the power density of the radiation in the visible range. A condenser lens collects the light which is transmitted by an optical fiber towards the spectrometer. The overall measurement of the spectrometer and the data from the two cameras can be combined to attempt to discriminate between the upward emission from outdoor lighting systems and the light reflected by lit surfaces.

A Command and Data Management Unit (CDMU) performs the on-board data handling. It is based on a Raspberry PI3. A custom developed application software based on Linux OS runs on it; figure 1 explains its functional scheme.

An on-board timer synchronizes and triggers the data-acquisition. The position of the system, the pointing retrieved by the GPS and Attitude and Heading Reference System (AHRS) are correlated with the acquired data. An on-board non-volatile memory stores the acquired data, which will be processed later on ground. A telemetry link allows communication between the CDMU and ground. Telecomands (TC) sent from ground can be used to configure the acquisition parameters. During the experiment the CDMU generates in real-time quick-look data, they are sent to the ground by Telemetry (TM). Those data include properly decimated and compressed images. On the basis of this information the user can check acquired data and consequently perform fine-tuning of the experiment. Figure 2 shows MINLU system on an octocopter drone.

III. CALIBRATION OF THE OPTICAL INSTRUMENTS

A picture of the multi-luminance meter and of the multi-spectrometer is presented in figure 3. We can see the CMOS cameras, the lenses, the photopic filter of the multi-luminance meter and the diffracting grid of the multi-spectrometer.

A. The multi-luminance meter

The image luminance meter is composed by a camera, its lens, and a photopic filter. The ensemble should have a spectral sensitivity as close as possible to the spectral sensitivity of the human eye, the function of which is presented by the red line of in figure 4 versus the wavelengths in the range the ensemble deals with. In the same figure the response of the camera sensor is presented too. It was decided to place the filter in front of the lens. I was considered a choice better than placing

Fig. 2. MINLU system on octocopter drone

the filter in contact with the camera sensor, as happens in some commercial cameras. The system analyzes the emission from sources far enough from it, therefore all rays collected by the frontal lens coming from a point in the framed scene can be supposed having the same direction. The deviation of the ray caused by a frontal filter can be neglected. On the contrary, the rays converging on a pixel of the sensor have different directions and their refraction on a filter placed close before the sensor would deteriorate the focus of the lens. A filter approximating the photopic function in the visible range was selected, it is the Omega Optical Photopic Filter. The response of the filter and of the camera sensor and the photopic filter are presented in figure 4 by the blue line and black dashed curve, respectively.

Neglecting the attenuation introduced by the lens, the response of the system is a good approximation of the photopic spectral

Fig. 3. The multi luminance meter (on the right) and the multi-spectrometer (on the left)

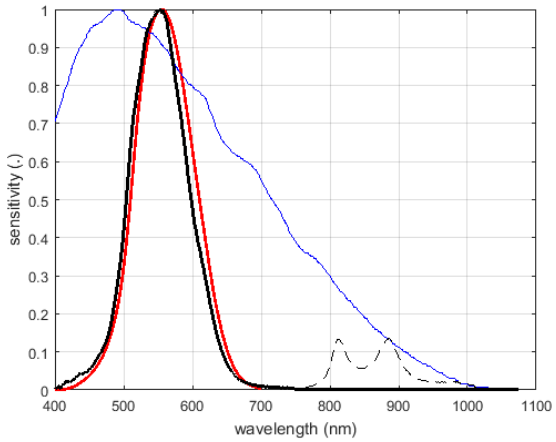

Fig. 4. Normalized spectral sensitivity of human eye (red), the camera (blue), camera with photopic filter (dashed black), overall system (thick black)

sensitivity of the human eye, in the visible range; the maximum error is equal to 6% of the peak value. Above 750 nm the response deviates significantly from the desired behavior. It has to be corrected to avoid different response of the system to the light coming from sources based on different technology. An additional low-pass filter was added to correct the response at longer wavelength. The final response is represented in figure 4 by the thicker back curve.

As reference in the calibration a spot luminance meter Konica Minolta LS-100 was used. Its uncertainty under Illuminant A is equal to 2% of the reading, if the resolution becomes negligible. The calibration of the multi-luminance meter is obtained under the light of a high-pressure sodium lamp. The calibrating coefficient is obtained equating the outputs of the multi-luminance meter and the spot luminance meter. Table II presents the luminance measures under different kind of light sources, three fluorescent lamps, a mercury vapor lamp and the high-pressure sodium lamp. The error is always less than 6% of the reading, which is considered small enough for our application. The last column presents the standard deviations on samples of 10 camera measures.

The vignetting, i.e. the reduction of the image brightness toward its periphery, is compensated. The system was placed on a goniometer [15] and characterized scanning its response for any lighting direction according to the procedure described in [16,17].

TABLE II. Luminance of a white target lit by lamps based on different technology: a spot luminance meter LS-100 is used as reference

Lamp	Ref. (cd m^{-2})	Camera (cd m^{-2})	Diff. (%)	Std (%)
Fluorescent 2600K	13.1	12.5	-5.6	1.3
Fluorescent 3750K	12.9	12.8	0.5	0.7
Fluorescent 5800K	12.5	12.4	-0.8	1.0
Mercury vapor	54.5	57.0	4.4	0.12
HP Sodium	82.1	82.1	0.02	1.0
HP Sodium calibration	61.0	61.0	0.00	0.15

B. The multi-spectrometer

The multi-spectrometer uses a monochromatic camera as the multi-luminance meter with an equal lens, furthermore a visible transmission diffracting grid with 300 groves/mm is paced in front of the lens. On the camera sensor, aside the image of each framed light source there is a recording of its spectral power density. Figure 5 shows the case when framing a group of street light sources, the image was recorded by an RGB camera for a better visual identification of the spectra. The choice of a low value of the groves/mm of the diffracting grid makes small the side shift of the first order spectrum with respect to the zero order. This last is the image of the light source. Therefore, the spectra of most of the framed sources appear within the sensor.

The distance between the image of the source and a point in the image of the spectrum represents the wavelength, but is not proportional to it. A calibration of the wavelength axis is required.

As discussed above for the multi-luminance meter, the sensitivity of the camera sensor depends on the wavelength; the same happens for the response of the diffracting grid. The value of the pixels covered by the spectra images are proportional to the power density at a specific wavelength, but the proportionality factor depends on the wavelength. A calibration of the amplitudes is required.

To calibrate the wavelength scale, a mercury vapor lamp is considered, its emission lines are well known and detectable. The expected FWHM of the equivalent filter of the multi-spectrometer is about 10 nm, therefore each mercury line is spread in a finite wavelength interval. Consequently, an uncertainty in the calibration could appear. To overcome this problem, the calibration of the wavelength axis was obtained comparing the multi-spectrometer data with the measurement from a calibrated spot spectrometer available in the laboratory. It is a Konica Minolta CS-1000 with a spectral bandwidth of 5 nm and an uncertainty on the wavelength values equal to 0.3 nm. The wavelength scale of the multi-spectrometer was adjusted minimizing the mean square difference between the measures of the power density provided by the two instruments. Before the comparison, the amplitudes of the data from the multi-spectrometer were corrected for the typical attenuation of the camera sensor and of the diffracting grid. Furthermore, the data from the CS-1000 were filtered to increase the equivalent bandwidth equating the FWHM of the multi-spectrometer. Figure 6 presents the two measures of the power distribution, the camera responsivity and diffracting grid attenuation normalized to their maximum. The wavelength scale of the multi-spectrometer was stretched and a good alignment of the peaks, corresponding to the mercury lines, appears. It can be observed the peak at about 406 nm shown by the CS-1000 is not detected by the multi-spectrometer. It could be due to a high attenuation introduced by the lens at the shortest wavelengths. This attenuation does not affect significantly the luminance measurements, at those wavelengths, in fact the sensitivity of the human eye and of the photopic filter present very low values, as it appears in figure 6.

In figure 6 it is apparent the amplitude attenuations due to the camera and the grid response are not compensated at some wavelengths. It could be mainly due to a very approximate knowledge of the diffracting grid. The calibration of the amplitude is obtained imposing the values measured by the reference spectrometer CS-1000. It was realized under a light with a continuous power density obtained as a mix of the outputs of an incandescent lamp and a white LED. As example of the effect of the amplitude calibration, figure 7 shows the power distribution of the light of a HP sodium lamp measured by the multi-spectrometer and the Konica Minolta CS-1000, the data series are normalized to their maxima. The curve corresponding to the multi-spectrometer shows a smoother behavior than the data from CS-1000. It is due to the wider FWHM of the equivalent filter of the multi-spectrometer. Furthermore, it is also caused by the finite apparent size of the analyzed reflecting source, even if very small.

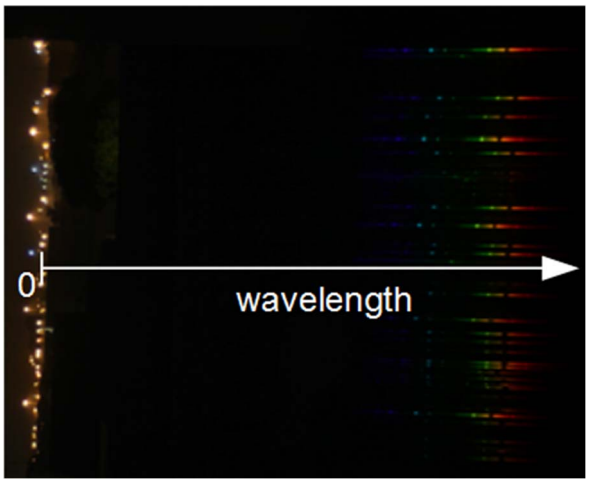

Fig. 5. Street light sources and their spectra. Image obtained on a camera sensor by placing the diffracting grid in fornt of the lens

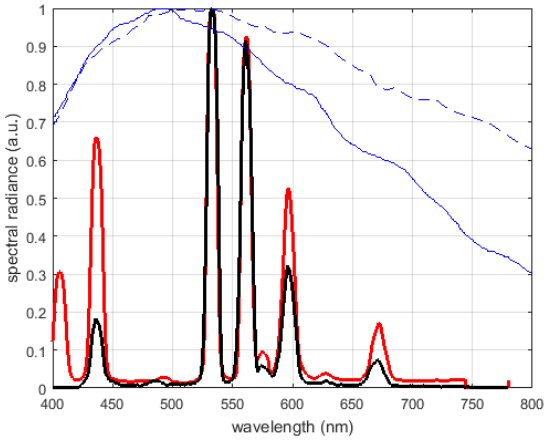

Fig. 6. Power distribution used for the wavelength calibration measured by the multi-spectrometer (black) and the Minolta CS-1000. In blue the camera sensitivity (continuous) and the diffracting grid attenuation (dashed), normalized to their maxima

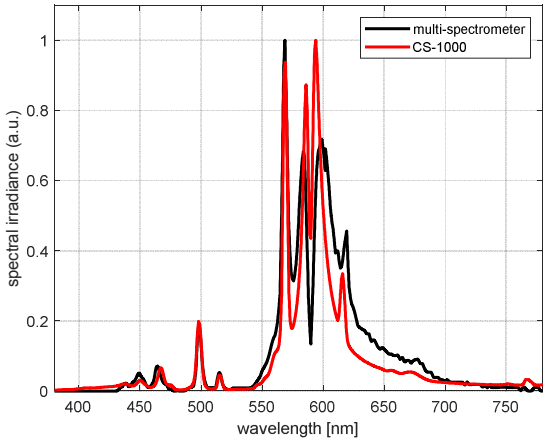

Fig. 7. Power distribution of a HP sodium lamp light measured by the multi-spectrometer (black) and the Minolta CS-1000 (red), the data series are normalized to their maxima

The compensation of the vignetting is applied also for the spectral measurements.

IV. Conclusions

The calibration of the proposed image suite allows measurements of the luminance and the power spectral density of the framed surfaces with an uncertainty comparable with those of industrial instruments. It allows to identify polluting sources quantifying their emission in terms of luminous intensity and therefore of importance in causing the artificial luminance of the sky. The system is able to discriminate among the different light sources used for street and outdoor lighting on the basis of the measurement of their power density with a good wavelength resolution. It significantly overcomes the measures obtained by satellites. The limited dimensions and weight of the unit permit the use on drones and tethered balloons to analyze upward emissions on a wide area and over several hours during the night, following the dimming of outdoor and street lights.

Acknowledgment

MINLU is developed under coordination and funding by Department of Industrial Engineering as part of the Twinning research program of the University of Padova.

References

[1] Reducing the ecological consequences of night-time light pollution: options and developments, Gaston et al. Journal of Applied Ecology 2012, 49, 1256–1266

[2] C. Elvidge, M. Imhoff, K. Baugh, V. Hobson, I. Nelson, J. Safran, J. Dietz, B. Tuttle, Night-time lights of the world: 1994 – 1995. ISPRS Journal of Photogrammetry and Remote Sensing 56, 81-99 (2001)

[3] A. Sánchez de Miguel, J. Zamorano, J. G. Castaño, S. Pascual, Evolution of the energy consumed by street lighting in Spain estimated with DMSP-OLS data. Journal of Quantitative Spectroscopy & Radiative Transfer 139 (2014), 109 – 117

[4] F.-C. Hsu, K. E. Baugh, T. Ghosh, M. Zhizhin, C. D. Elvidge, DMSP-OLS radiance calibrated nighttime lights time series with intercalibration, Remote Sensing 7 (2015), 1855-1876

[5] X. Li, Y. Zhou, A stepwise calibration of global DMSP/OLS stable nighttime light data (1992-2013), Remote Sensing 9 (2017), 637

[6] S. D. Miller, W. Straka, S. P. Mills, C. D. Elvidge, T. F. Lee, J. Solbrig, A. Walther, A. K. Heidinger, S. C. Weiss, Illuminating the capabilities of the Suomi National Polar-Orbiting Partnership (NPP) Visible Infrared Imaging Radiometer Suite (VIIRS) day/night band, Remote Sensing 5, 6717 – 6766 (2013).

[7] Miller, S.D.; Straka, W.; Mills, S.P.; Elvidge, C.D.; Lee, T.F.; Solbrig, J.; Walther, A.; Heidinger, A.K.; Weiss, S.C. Illuminating the capabilities of the suomi national polar-orbiting partnership (NPP) visible infrared imaging radiometer suite (VIIRS) day/night band, Remote Sensing (2013), 5, 6717–6766

[8] A. Barducci, P. Marcoionni, I. Pippi, and M. Poggesi, Effects of light pollution revealed during a nocturnal aerial survey by two hyperspectral imagers, Applied Optics 42, Issue 21 (2003), 4349-4361

[9] Kuechly, H.U.; Kyba, C.C.M.; Ruhtz, T.; Lindemann, C.; Wolter, C.; Fischer, J.; Holker, F. Aerial survey and spatial analysis of sources of light pollution in Berlin, Germany. Remote Sensing Environ 126 (2012), 39–50

[10] Hale JD, Davies G, Fairbrass AJ, Matthews TJ, Rogers CDF, et al. (2013), Mapping Lightscapes: Spatial Patterning of Artificial Lighting in an Urban Landscape. PLoS ONE 8(5): e61460. doi:10.1371/journal.pone.0061460

[11] Miller, S.D.; Straka, W.; Mills, S.P.; Elvidge, C.D.; Lee, T.F.; Solbrig, J.; Walther, A.; Heidinger, A.K.; Weiss, S.C. Illuminating the capabilities of the suomi national polar-orbiting partnership (NPP) visible infrared imaging radiometer suite (VIIRS) day/night band, Remote Sensing (2013), 5, 6717–6766

[12] C. C. M. Kyba, S. Garz, H. Kuechly, A. Sánchez de Miguel, J. Zamorano, J. Fischer, F. Hölker, High-resolution imagery of Earth at night: New sources, opportunities and challenges, Remote Sensing 7, 1 – 23 (2015)

[13] R. Estrada-García, M. García-Gil, L. Acosta, S. Bará, A. Sanchez de Miguel, J. Zamorano, Statistical modelling and satellite monitoring of upward light from public lighting, Lighting Research and Technology 48 (2016)

[14] P. Fiorentin, C. Bettanini, E. Lorenzini, A- Aboudan, G. Colombatti, S. Ortolani & A. Bertolo, MINLU: An Instrumental Suite for Monitoring Light Pollution from Drones or Airballoons, 5th IEEE International Workshop on Metrology for AeroSpace (MetroAeroSpace), 274-278, June 2018

[15] P. Fiorentin, A. Scroccaro, Analysis of the Performance of a Goniometer for Studying Surface Reflection, IEEE Transactions on Instrumentation and Measurement, Vol. 57, N. 11,(2008), 2522 - 2527

[16] P. Fiorentin, P. Iacomussi, G. Rossi, Characterization and calibration of a CCD detector for light engineering, IEEE Transaction on Instrumentation and Measurement, Vol. 54, N. 1, (2005), 171-177

[17] P. Fiorentin, A,. Scroccaro, Detector-Based Calibration for Illuminance and Luminance Meters - Experimental Results, 171-177, I IEEE Transaction on Instrumentation and Measurement, vol.59 (2010), 1375-1381